As a next step the PMD compensator was inserted. The controller maximised the 25 and 40GHz power levels. The autocorrelation trace reveals a slightly narrower pulse with a deconvolved 5.2ps width (Fig. 2*b*). Similar pulse peaking has already been found in NRZ experiments [3, 6, 8]. Then the emulator was inserted with 10 + 6ps of DGD in the PMF pieces. The deconvolved pulsewidth was now 5.4ps but the autocorrelation pedestal (3% back-to-back) increased to 7.5% (Fig. 2*c*). With 10 + 10ps of DGD in the emulator the deconvolved pulsewidth was 5.8ps and the pedestal 12% (Fig. 2*d*). However, the autocorrelation function exaggerates the true pedestal, as may be seen from a fitted calculation result assuming the superposition of two Gaussian pulses (Fig. 2*e*). There is very little intersymbol interference. For comparison we give also an autocorrelation trace for the emulator plus compensator with the control signals minimised rather than maximised. In this case the original pulses essentially disappear due to PMD (Fig. 2*f*).

A dynamic measurement was made with the 10 + 6ps emulator and the compensator. Starting from an initial standstill the motorised fibre polarisation transformers were made to turn successively faster.

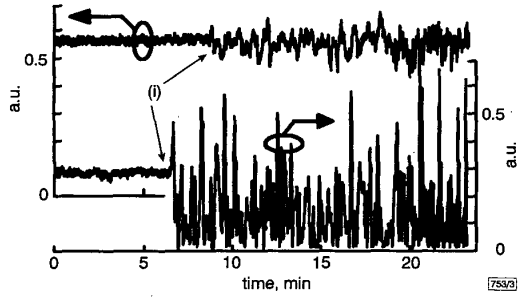

Fig. 3 *Recorded spectral power*

Top trace: control on
Bottom trace: control off
(i) eight fibre coils in emulator start turning

Fig. 3 (upper trace) shows an aggregate control signal obtained by linearly combining the 40 and 25GHz power level signals. Part of the signal variations can be attributed to polarisation dependence (~1dB) of the components following the compensator. For a comparison the measurement was repeated when the control was off. Large signal fluctuations occurred as expected when the fibre coils started to turn (Fig. 3, lower trace). The experiment shows that optical PMD compensation with a simple, purely electrical PMD detection scheme is also possible for RZ signals.

Conclusions: For the first time to our knowledge, the PMD of RZ signals has been compensated. A distributed $LiNbO_3$ PMD compensator was used to equalise 6ps, 40Gbit/s pulses distorted by 10 + 10ps of DGD, using a 10GHz modelocked Ti:Er:$LiNbO_3$ waveguide laser.

Acknowledgment: Development of the integrated-optical PMD compensator was funded by Siemens AG, Munich, Genuany. Development of the modelocked laser was funded in ACTS project ESTHER and HNI-Project (Univ. Paderborn).

22nd April 1999

Electronics Letters Online No: 19990827

DOI: 10.1049/el:19990827

S. Hinz, D. Sandel, M. Yoshida-Dierolf, V. Mirvoda and R. Noé (*Optical Communications and High-Frequency Engineering, University of Paderborn, Warburger Strasse 100, 33098 Paderborn, Germany*)

G. Feise, H. Herrmann, R. Ricken, W. Sohler, H. Suche, F. Wehrmann and R. Wessel (*Applied Physics, University of Paderborn, Warburger Strasse 100, 33098 Paderborn, Germany*)

R. Noé: Corresponding author

E-mail: noe@uni-paderborn.de

References

1 TAKAHASHI, T, IMAI, T., and AIKI, M..: 'Automatic compensation technique for timewise fluctuating polarisation mode dispersion in in-line amplifier systems', *Electron. Lett.*, 1994, **30**, (4), pp. 348–349

2 HEISMANN, F., FISHMAN, D.A., and WILSON, D.L.: 'Automatic compensation of first order polarization mode dispersion in a 10Gb/s transmission system'. ECOC '98, Madrid, Spain, 1998, Paper WdC11

3 SANDEL, D., YOSHIDA-DIEROLF, M., NOÉ, R., SCHÖPFLIN, A., GOTTWALD, E., and FISCHER, G.: 'Automatic polarisation mode dispersion compensation in 40Gbit/s optical transmission system', *Electron. Lett.*, 1998, **34**, (23), pp. 2258–2259

4 CHBAT, M.W., SOIGNÉ, J.-P., FUERST, T., ANTHONY, J.T., LANNE, S., FÉVRIER, H., DESTHIEUX, B.M., BUSH, A.H., and PENNINCKX, D.: 'Long term field demonstration of optical PMD compensation on all installed OC-192 link'. OFC/IOOC '99, San Diego, 21–26 February 1999, Paper PD12

5 OOI, H., AKIYAMA, Y., and ISHIKAWA, G.: 'Automatic polarization-mode dispersion compensation in 40Gbit/s transmission'. OFC/IOOC '99, San Diego, 21–26 February 1999, Paper WE5

6 NOÉ, R., SANDEL, D., YOSHIDA-DIEROLF, M., HINZ, S., GLINGENER, C., SCHEERER, C., SCHÖPFLIN, A., and FISCHER, G.: 'Polarisation mode dispersion compensation at 20Gbit/s with fibre-based distributed equaliser', *Electron. Lett.*, 1998, **34**, (25), pp. 2421–2422

7 NOÉ, R., SANDEL, D., HINZ, S., YOSHIDA-DIEROLF, M., MIROVDA, V., FEISE, G., HERRMANN, H., RICKEN, R., SOHLER, W., WEHRMANN, F., GLINGENER, C., SCHÖPFLIN, A., FÄRBERT, A., and FISCHER, G.: 'Integrated optical $LiNbO_3$ distributed polarisation mode dispersion compensator in 20Gbit/s transmission system', *Electron. Lett.*, 1999, **35** , (8), pp. 652–654

8 JOPSON, R.M., NELSON, L.E., PENDOCK, G.J., and GNAUCK, A.H.: 'Polarization-mode dispersion impairment in return-to-zero and nonreturn-to-zero systems'. OFC/IOOC '99, San Diego, 21–26 February 1999, Paper WE3

9 WESSEL, R., RICKEN, R., ROCHAUSEN, K., SUCHE, H., and SOHLER, W.: '10GHz mode locked Ti:Er:$LiNbO_3$ waveguide laser with coupled cavity: super mode selection and pulse repetition rate doubling'. Proc. 9th European Conf. on Integrated Optics (ECIO'99), Turin, Italy, 14–16 April 1999, Paper ThE1

Spectral encoding and decoding of 10Gbit/s femtosecond pulses using high resolution arrayed-waveguide grating

H. Tsuda, H. Takenouchi, T. Ishii, K. Okamoto, T. Goh, K. Sato, A. Hirano, T. Kurokawa and C. Amano

A 10Gbit/s, 810fs, return-to-zero signal is spectrally encoded, transmitted over a 40km dispersion shifted fibre, and decoded using a photonic spectral encoder and decoder pair that uses high resolution arrayed-waveguide gratings and phase filters. A 255 bit binary phase code with the maximum length sequence is used for spectral coding.

Introduction: A combination of optical code division multiplexing (OCDM) with time division multiplexing (TDM) and wavelength division multiplexing (WDM) improves the signal spectrum efficiency and flexibility of fibre optic communication systems. A photonic encoder/decoder pair is one of the key components of such an optical CDM system. Studies have been made on encoding and decoding optical pulses through the use of diffraction grating pairs [1, 2] and optical transversal filters [3]. These diffraction grating systems, however, do not have sufficient spectral resolution for high signal spectrum efficiency, while optical transversal filters are not easy to use with WDM systems. In this Letter we describe a photonic spectral encoder and decoder pair [4] that uses high-resolution arrayed-waveguide gratings (AWGs).

Configuration and operating principle of spectral encoder/decoder: We used a reflection-type AWG, which is polarisation insensitive, and a spatial phase filter on the spectral plane, as shown in Fig. 1. This configuration can also be used for other photonic signal processing operations, including dispersion compensation and

phase-shift keying direct detection [5 – 7]. The AWG encoder spectrally decomposes the input pulses into their frequency components, modulates each phase with the encoding filter, and reforms the waveform. Binary phase encoding with the maximum length sequence (M-sequence) is used. The spectral bit width was set at $1/(T_{WD}$, timeslot). The phase function of the filter, $H_M(\omega)$, is written as

$$H_M(\omega) = \exp[i\pi M_k(\Omega(\omega))] \quad (1)$$

$$\Omega(\omega) = \frac{\omega - \omega_0}{\delta\omega} \bmod (2^k - 1) \quad (2)$$

where $M_k(x)$ is the xth element of the k stage M-sequence, ω is the angular frequency, ω_0 is the centre frequency of the AWG and $\delta\omega$, which is $1/(T_{WD}$, timeslot), is the bit width of the filter. The output waveform from the AWG encoder is described approximately as

$$\{f(\tau)e^{i\omega_0\tau}\} * h_M(\tau) \quad (3)$$

where $f(\tau)$ is the input pulse waveform and $h_M(\tau)$ is the Fourier transform of $H_M(\omega)$. The M-sequence is a pseudorandom sequence, so the output waveform is spread out within the timeslot without a clear peak. After transmission with dispersion compensation, the signal is again spectrally modulated by the AWG decoder, which has the same filter. The waveform output from the AWG decoder is given by

$$\{f(\tau)e^{i\omega_0\tau}\} * F\{H_M(\omega)H_M(\omega')\} \ (F\text{: Fourier transform}) \quad (4)$$

When $\Omega(\omega) = \Omega(\omega')$, $H_M(\omega)H_M(\omega') = 1$ and $f(\tau)$ is recovered. When $\Omega(\omega) \neq \Omega(\omega')$, $H_M(\omega)H_M(\omega') = H_M(\omega'')$ and the output waveform duplicates random noise. Therefore, the pulse is recovered only when the spectral positions of the encoding filter and the decoding filter are equivalent.

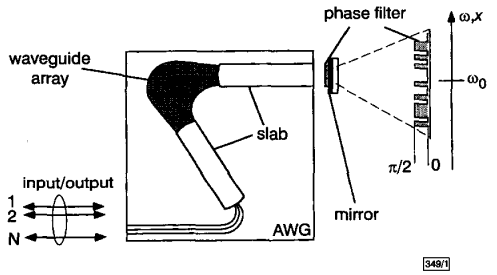

Fig. 1 *Configuration of photonic spectral encoder/decoder*

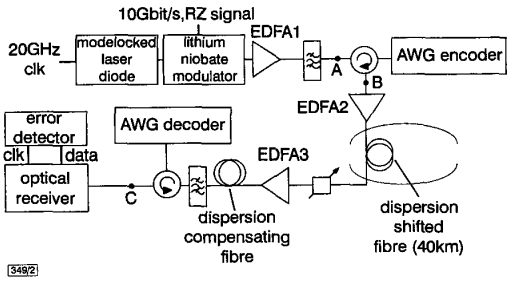

Fig. 2 *Experimental setup for spectral encoding and decoding*

Experiment: The experimental setup is shown in Fig. 2. A modelocked laser diode [8] with a repetition frequency of 20GHz and a centre wavelength of 1549nm was used for the light source. A 10Gbit/s, return-to-zero (RZ) signal was generated by a lithium niobate (LN) intensity modulator. The width of the pulse input to the AWG encoder was 810fs after compensation of the second-order dispersion. The pulsewidth was measured by an autocorrelator under the assumption that the waveform was Gaussian. The diffraction order of the AWG was 72 and the array had 286 waveguides. The spatial dispersion was 1.5GHz/μm and the resolution was 12.6GHz. The spatial phase filter was fabricated by electron beam lithography of a polymethiglutarimide (PMGI) thin film on an Au mirror; its phase accuracy was ~π/15. An M-sequence with a length of 255 bits was used. The one bit width of the filter was 6.7μm, which corresponds to 10GHz. The spectrally encoded 10Gbit/s, RZ, 2^{23}–1 PRBS signal was launched into the 40km dispersion shifted fibre (DSF), the total dispersion of which was +6.6ps/nm, and then to the dispersion compensating fibre (DCF), decoded by the AWG decoder, and received.

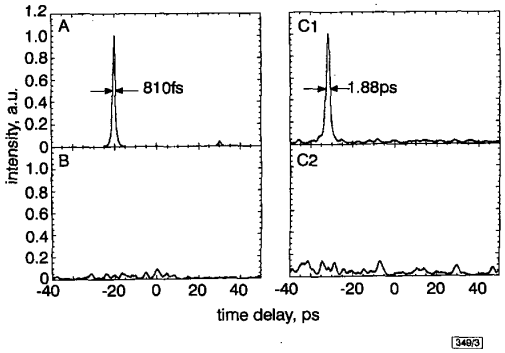

Fig. 3 *Waveforms at points (A), (B) and (C) in Fig. 2*

A: input waveform
B: encoded waveform
*C*1: correctly decoded waveform
*C*2: incorrectly decoded waveform

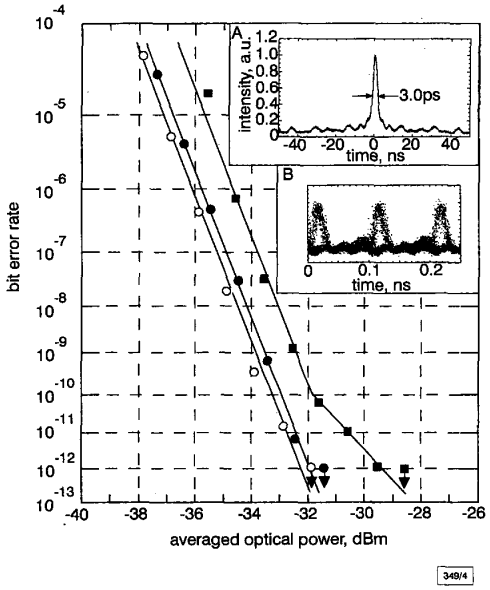

Fig. 4 *BER performance of AWG encoder/decoder*

○ back-to-back configuration
● after transmission with launching power of 5dBm
■ after transmission with launching power of 10dBm
Inset *A*: autocorrelation of decoded pulse after 40km transmission
Inset *B*: received eye pattern

Results and discussion: Waveforms at points A, B, and C in Fig. 2 were measured by a cross-correlator after dispersion compensation, as shown in Fig. 3*A*, *B*, *C*1 and *C*2. The decoded waveform in the back-to-back configuration *C*1 had a clear peak with a width of 1.88ps when the decoding filter was in the correct position. In contrast, the decoded waveform *C*2 had no clear peak when the position of the decoding filter was shifted by an amount over 2 bits. These results indicate that the proposed spectral encoder and decoder basically work well. To confirm the feasibility of the AWG spectral encoder and decoder, bit error rates (BERs) were measured.

The decoded signal was received by a conventional 10Gbit/s optical receiver. The BERs were measured against the averaged optical power to EDFA3, as shown in Fig. 4. The open circles, closed circles, and closed squares, respectively, show BERs for a back-to-back configuration, after transmission with launching powers (P_{in}) of 5 and 10dBm. There was no significant sensitivity

penalty up to a P_{in} of 5dBm. Error-free (BER < 10^{-12}) transmission was successfully achieved when P_{in} < 10dBm. A high launching power to the DSF with very low dispersion was acceptable because the encoded pulse energy was spread over the time slot. Inset A shows the autocorrelation of the decoded pulse after 40km transmission with an autocorrelation width of ~3ps. A clear eye opening was observed, as shown in Inset B.

Conclusion: Error-free encoding and decoding of a 10Gbit/s RZ, 2^{23}–1 PRBS signal through a 40km transmission fibre was successfully demonstrated using the AWG spectral encoder and decoder pair. The encoder and decoder pair can be used in optical CDM systems with ultra-high-speed optical thresholders.

Acknowledgment: The authors are grateful to H. Iwamura and S. Mitachi of NTT Photonics Laboratories for their encouragement during this work.

31 March 1999

Electronics Letters Online No: 19990783

DOI: 10.1049/el:19990783

H. Tsuda, H. Takenouchi, T. Ishii and C. Amano (*NTT Photonics Laboratories, 3-1 Morinosato-Wakamiya, Atsugi, Kanagawa, 243-0198 Japan*)

E-mail: tsuda@aecl.ntt.co.jp

K. Okamoto and T. Goh (*NTT Photonics Laboratories, 162 Shirakata-Shirane, Tokai, Ibaragi, 319-1196 Japan*)

K. Sato and A. Hirano (*NTT Network Innovation Laboratories, 1-1 Hikari-no-oka, Yokosuka, Kanagawa, 239-0847 Japan*)

T. Kurokawa (*Tokyo University of Agriculture & Technology, 2-24-16 Nakamachi, Koganei, Tokyo, 184-8588 Japan*)

References

1 SALEHI, J.A., WEINER, A.M., and HERITAGE, J.P.: 'Coherent ultrashort light pulse code-division multiple access communication systems', *J. Lightwave Technol.*, 1990, **8**, (3), pp. 478–491

2 SARDESAI, H.P., CHANG, C.-C., and WEINER, A.M.: 'A femtosecond code-division multiple-access communication system test bed', *J. Lightwave Technol.*, 1998, **16**, (11), pp. 1953–1964

3 CORNWELL, W.D., WADA, N., KITAYAMA, K.-I., and ANDONOVIC, I.: 'Experimental demonstration of coherent coding of picosecond pulses', *Electron. Lett.*, 1998, **34**, (2), pp. 204–205

4 TSUDA, H., TAKENOUCHI, H., ISHII, T., OKAMOTO, K., GOH, T., SATO, K., HIRANO, A., KUROKAWA, T., and AMANO, C.: 'Photonic spectral encoder/decoder using an arrayed-waveguide grating for coherent optical code division multiplexing'. Tech. Dig. Optical Fiber Communication Conf. (OFC), 1999, Paper PD32

5 TSUDA, H., KUROKAWA, T., OKAMOTO, K., ISHII, T., NAGANUMA, K., INOUE, Y., and TAKENOUCHI, H.: 'Second- and third-order dispersion compensation using a high resolution arrayed-waveguide grating'. Tech. Dig. European Conf. Optical Communication (ECOC), 1998, Paper WdC13, pp. 533–534

6 TAKENOUCHI, H., TSUDA, H., AMANO, C., GOH, T., OKAMOTO, K., and KUROKAWA, T.: 'An optical phase-shift keying direct detection receiver using a high-resolution arrayed-waveguide grating'. Tech. Dig. Optical Fiber Communication Conf. (OFC), 1999, Paper TuO4

7 KUROKAWA, T., TSUDA, H., OKAMOTO, K., NAGANUMA, K., TAKENOUCHI, H., INOUE, Y., and ISHII, M.: 'Time-space-conversion optical signal processing using arrayed-waveguide grating', *Electron. Lett.*, 1997, **33**, (22), pp. 1890–1891

8 SATO, K., WAKITA, K., KOTAKA, I., KONDO, Y., YAMAMOTO, M., and TAKADA, A.: 'Monolithic strained-InGaAsP multiple-quantum-well lasers with integrated electroabsorption modulators for active mode locking', *Appl. Phys. Lett.*, 1994, **65**, (1), pp. 1–3

Developing holey fibres for evanescent field devices

T.M. Monro, D.J. Richardson and P.J. Bennett

The overlap of the optical mode in a holey fibre with the air holes is calculated for the first time. This is achieved using a vector modal decomposition approach. It is shown that a significant fraction of the modal power can be made to overlap with the holes, which suggests that these unusual fibres may be useful as evanescent field devices.

Introduction: Holey optical fibres (HFs) have a cladding region comprised of air holes running along the full length of the fibre (see Fig. 1). One example of an HF is a photonic crystal fibre (PCF), in which the holes are arranged periodically. HFs guide light due to the effective refractive index difference between the core (a missing hole) and the cladding. Altering the hole arrangement can radically change the properties of HFs, and investigations to date have explored modal profiles, mode area and dispersion [1, 2]. The unusual properties of HFs arise from the strong wavelength dependence of the effective cladding index n_{cl}; at longer wavelengths the field extends further into the holes, reducing n_{cl}. As a consequence, some HFs can be singlemoded regardless of the wavelength [1].

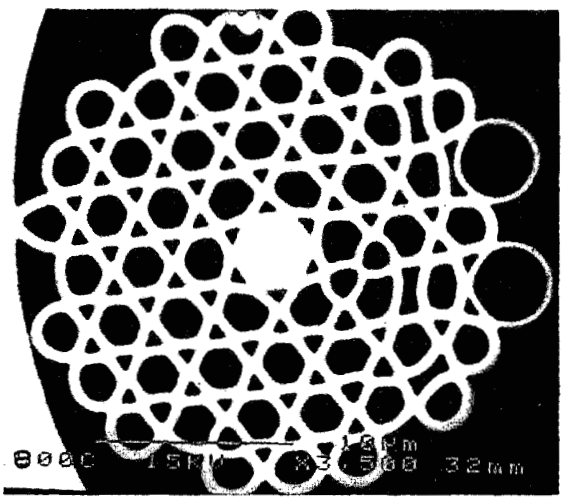

Fig. 1 *SEM of typical large air fill HF*
$d/\Lambda \simeq 0.6$, $\Lambda \simeq 3.2\mu m$

In [2] we developed a scalar orthogonal function method for HFs, which is valid when the holes are small. We have also extended this to the vector case, which enables us to explore the full range of HFs. This technique involves decomposing the modal field using localised functions. The central index defect and the air hole lattice are described independently using localised functions for the defect and periodic functions for the holes. This can be efficient and accurate because the quantities are described by functions chosen carefully to suit.

The holes in HFs open up new opportunities for exploiting the interaction of light with gases and liquids via evanescent field effects. For example, the concentration of pollutants in a gas could be determined by measuring the absorption which occurs as light propagates through the gas for a range of wavelengths [3]. We show that the HF geometry can naturally provide extremely long optical path lengths.

Overlap with holes: To assess the suitability of HFs for evanescent field devices, it is crucial to know the magnitude of the overlap of the modal field with the holes, and here we present what we believe to be the first such calculations. We define PF_{holes} to be the fraction of the fundamental mode's power which is located in the holes. First the mode profile for a given wavelength is calculated using the full vector model. It is then straightforward to evaluate PF_{holes} at this wavelength numerically, and we have calculated PF_{holes} for a range of different HFs.